

The Geometry of Thought: How Scale Restructures Reasoning in Large Language Models

Samuel Cyrenius Anderson*

1. Scrivly.AI

* sam@scrivly.ai

Abstract

Scale does not uniformly improve reasoning—it restructures it. Analyzing 25,000+ chain-of-thought trajectories across four domains (Law, Science, Code, Math) and two scales (8B, 70B parameters), we discover that neural scaling laws trigger domain-specific phase transitions rather than uniform capability gains.

Legal reasoning undergoes *Crystallization*: 45% collapse in representational dimensionality (d_{95} : $501 \rightarrow 274$), 31% increase in trajectory alignment, and $10 \times$ manifold untangling. Scientific and mathematical reasoning remain

Liquid—geometrically invariant despite $9 \times$ parameter increase. Code reasoning forms a discrete *Lattice* of strategic modes (silhouette: $0.13 \rightarrow 0.42$).

This geometry predicts learnability. We introduce Neural Reasoning Operators—learned mappings from initial to terminal hidden states. In crystalline legal reasoning, our operator achieves 63.6% accuracy on held-out tasks via probe decoding, predicting reasoning endpoints without traversing intermediate states.

We further identify a universal oscillatory signature (coherence ≈ -0.4) invariant across domains and scales, suggesting attention and feedforward layers drive reasoning through opposing dynamics.

These findings establish that the cost of thought is determined not by task difficulty but by manifold geometry—offering a blueprint for inference acceleration where topology permits.

1 Introduction

The scaling hypothesis has become the central organizing principle of modern deep learning: larger models, trained on more data, yield predictably better performance across an expanding frontier of tasks. Neural scaling laws formalize this intuition, demonstrating that loss decreases as a power law in model parameters, dataset size, and compute budget [25, 27]. For reasoning tasks specifically, chain-of-thought (CoT) prompting has revealed that scale unlocks qualitatively new capabilities—arithmetic, symbolic manipulation, and multi-hop inference—that smaller models cannot perform regardless of prompting strategy [57].

Yet the scaling hypothesis, as typically articulated, is silent on a crucial question: *how does scale improve reasoning?* The default assumption is that larger models simply “know more”—that additional parameters encode additional facts, patterns, or heuristics that accumulate to produce better outputs. Under this view, scaling is purely quantitative: more of the same, executed more reliably.

This paper presents evidence for a sharply different picture. We demonstrate that scale does not merely improve reasoning—it restructures it, triggering qualitative geometric reorganizations in how models represent the reasoning process itself. Moreover, these reorganizations are domain-dependent: the same $9 \times$ increase in parameters induces dramatically different effects depending on what the model is reasoning about. This paper asks a deliberately sharp question:

Is reasoning inherently a path, or can it be treated as an endpoint computation?

The question is not about whether intermediate text is useful, nor whether verbalized CoT is a faithful transcript of internal computation. Rather, it asks whether the internal evolution of model representations during reasoning exhibits sufficient geometric regularity that the *endpoint* of that evolution can be predicted without explicitly simulating every intermediate step.

1.1 The dynamical view: reasoning as trajectories

We adopt a dynamical systems perspective on transformer computation. Let $h_t \in \mathbb{R}^d$ denote the final-layer hidden state at token position t during chain-of-thought generation. A *reasoning trajectory* is the sequence

$$\tau = (h_0, h_1, \dots, h_T) \tag{1}$$

traced through representation space as the model generates intermediate reasoning text. While the underlying computation is history-dependent (attention conditions on all previous tokens), the observed hidden states are points in a fixed-dimensional space whose geometric properties can be measured and compared.

This perspective transforms abstract questions about “reasoning capability” into concrete questions about manifold structure: What is the effective dimensionality of reasoning trajectories? Do trajectories align toward canonical pathways or diffuse through high-dimensional space? Do distinct reasoning strategies cluster into separable modes? How do these geometric properties change with scale?

Prior work in mechanistic interpretability has begun characterizing such structure. Li et al. (2025) formalize a “reasoning manifold” and use geometric deviation to diagnose failures [32]. Carson and Reisizadeh (2025) model sentence-level trajectories as drift-diffusion processes with regime switching [10]. Marin (2024) proposes phase-space analysis of multi-hop reasoning [38]. However, these approaches are primarily diagnostic—they identify geometric signatures *post hoc* but do not systematically investigate how geometry varies across domains or scales.

We extend this program by treating trajectory geometry as an independent variable. Concretely, we extract hidden-state trajectories during chain-of-thought generation across four reasoning domains (Law, Science, Code, Math) and two model scales (Llama-3-8B-Instruct and Llama-3.1-70B-Instruct), quantify their geometric properties using a standardized measurement suite, and test whether the resulting structure supports learned operators that can predict terminal hidden states without traversing full trajectories.

1.2 A geometric measurement suite

We introduce four complementary metrics to characterize reasoning geometry:

- **Global dimension (d_{95}):** the number of principal components required to capture 95% of variance in the trajectory point cloud—the effective linear dimensionality of the reasoning manifold.
- **Intrinsic dimension (d_{mle}):** the Levina–Bickel maximum likelihood estimate of local manifold dimension, capturing nonlinear structure that PCA may miss.
- **Trajectory alignment:** the mean cosine similarity between individual displacement vectors ($h_T - h_0$) and the population mean displacement direction. High alignment indicates convergence toward a canonical reasoning pathway; low alignment indicates diffuse, exploratory dynamics.

- **Step-to-step coherence:** the mean cosine similarity between successive velocity vectors $v_t = h_{t+1} - h_t$ and v_{t+1} . Positive coherence indicates smooth flow; negative coherence indicates oscillatory “zig-zag” dynamics.

Additionally, we compute silhouette scores to quantify clustering into discrete modes, and the global-to-local dimension ratio (G/L) to measure manifold “tangling”—whether the representation is folded complexly through ambient space or lies comparatively flat.

1.3 From geometry to operators: the amortization hypothesis

Our geometric analysis is not merely descriptive. We propose an *amortization hypothesis*: if reasoning trajectories exhibit favorable geometry—low intrinsic dimension, high alignment, and clear clustering—then the endpoint of reasoning may be predictable without explicitly simulating every intermediate step. We define the endpoint operator

$$\mathcal{F}_c : h_0 \mapsto h_T \quad (2)$$

that maps initial hidden states to terminal hidden states under context c .

Unlike speculative decoding or draft-and-verify approaches—which remain fundamentally token-anchored and reduce constant factors in traversing a reasoning path—endpoint prediction targets a different axis entirely: whether the $O(T)$ sequential dependence can be bypassed at operator evaluation time when geometry permits.

To evaluate whether a predicted terminal state is *functionally* informative, we consider two decoding regimes. (i) **Frozen-unembedding decoding** applies the model’s original, unmodified output head (unembedding) directly to h_T with no trained decoder, serving as a stringent diagnostic of whether the operator lands in the model’s native coordinate frame. (ii) **Decoder-adapter (probe) decoding** trains a lightweight adapter to map predicted states to answer-token logits (Section 3.5.2). Unless stated otherwise, all reported “decoding accuracy” in this paper refers to the adapter/probe regime; frozen-unembedding decoding is treated as a diagnostic and is not used as the headline accuracy metric in our experimental setting.

1.4 Preview of findings: a phase diagram of thought

Our experiments reveal that reasoning geometry is not uniform across domains, and that scale induces domain-specific phase transitions rather than universal improvement. We identify three distinct geometric phases:

Crystallization (Law). Legal reasoning undergoes a dramatic structural transformation between 8B and 70B parameters. Global dimensionality collapses by 45% ($d_{95} : 501 \rightarrow 274$), trajectory alignment increases by 31% ($0.72 \rightarrow 0.94$), and the global-to-local ratio drops from $\sim 10\times$ to $\sim 1\times$, indicating complete manifold “untangling.” The model does not merely reason *better* about law at scale—it reasons *differently*, compressing the space of possible reasoning pathways into a low-dimensional, highly reproducible structure. We term this phase *Crystalline*: rigid, ordered, and geometrically efficient.

Liquidity (Science, Math). In sharp contrast, scientific and mathematical reasoning exhibit scale invariance. Despite a $9\times$ parameter increase, global dimensionality remains unchanged (Science: $237 \rightarrow 235$; Math: $501 \rightarrow 501$), and manifold structure shows no significant reorganization. These domains maintain diffuse, exploratory geometry at both scales—a *Liquid* phase that resists compression. Scale provides more parameters but does not simplify the representational structure of scientific thought.

Lattice formation (Code). Programming tasks reveal a third phase characterized by discrete modularity. Code reasoning achieves the highest clustering quality

(silhouette: 0.42) while maintaining moderate alignment, suggesting that scale organizes programming into well-separated strategic modes—a *Lattice* of distinct problem-solving approaches rather than convergence to a single pathway.

Beneath this domain-specific variation, we observe a universal dynamical signature: step-to-step coherence remains approximately -0.4 across all domains and scales. This negative coherence indicates that transformer reasoning is inherently oscillatory—trajectories “zig-zag” through representation space rather than flowing smoothly toward attractors. Neither domain nor scale modulates this signature, suggesting it reflects an architectural invariant of transformer dynamics rather than a property of reasoning content.

Finally, pilot validation with Neural Reasoning Operators demonstrates that geometric structure predicts operator learnability. Our **Turbo** operator—a nonlinear architecture conditioned on the initial velocity vector ($h_1 - h_0$)—achieves 74.7% latent similarity and 63.6% decoding accuracy on legal classification tasks when evaluated on held-out trajectories, exceeding baselines by 10 percentage points. This confirms that the geometry of reasoning is not merely descriptive but functionally predictive: favorable manifold structure enables amortized inference at operator evaluation time, even though the training trajectories were generated via standard CoT.

1.5 Contributions

This paper makes the following contributions:

1. **Domain-dependent scaling laws (geometric).** We provide systematic evidence that neural scaling laws operate differently across reasoning domains at the geometric level. Scale triggers Crystallization in rule-governed domains (Law), leaves exploratory domains invariant (Science, Math), and induces Lattice formation in compositional domains (Code).
2. **A geometric taxonomy of reasoning.** We introduce and empirically validate a three-phase classification—Crystalline, Liquid, and Lattice—that characterizes reasoning structure in terms of dimensionality, alignment, and clustering rather than task accuracy alone.
3. **The universal oscillatory signature.** We identify a domain- and scale-invariant dynamical pattern (coherence ≈ -0.4) that appears fundamental to transformer reasoning, providing a new empirical constraint for theories of autoregressive computation.
4. **Geometry-aware operator learning.** We demonstrate that trajectory geometry predicts the feasibility of amortized inference. Our Turbo operator leverages initial velocity to predict terminal states in crystalline domains, achieving 63.6% accuracy on held-out legal reasoning tasks.
5. **A reproducible measurement framework.** We release a standardized geometric measurement suite and extraction pipeline enabling systematic comparison of reasoning structure across models, scales, and domains.

Taken together, these results suggest that the “cost of thought” is not an immutable property of task difficulty, but a function of the geometry of the reasoning manifold—a geometry that varies dramatically across domains and that scale reshapes in domain-specific ways. Understanding this geometry may be essential for predicting emergent capabilities, designing efficient inference systems, and ensuring reliable deployment of reasoning models in high-stakes applications.

2 Related Work

Our work sits at the intersection of several research programs: neural scaling laws, chain-of-thought reasoning, mechanistic interpretability, the manifold hypothesis, phase transitions in neural networks, inference acceleration, and operator learning. We review each in turn, positioning our contributions relative to existing findings.

2.1 Neural Scaling Laws

The empirical study of neural scaling laws has become foundational to modern deep learning practice. Kaplan et al. (2020) [27] established that language model loss decreases as a power law in model parameters, dataset size, and compute budget, with remarkably consistent exponents across seven orders of magnitude. Hoffmann et al. (2022) [25] refined these laws with the “Chinchilla” scaling analysis, demonstrating that optimal compute allocation requires scaling data and parameters in tandem, and that many large models are substantially undertrained relative to their parameter count.

Subsequent work has extended scaling analysis beyond aggregate loss. Wei et al. (2022b) [56] documented “emergent abilities”—capabilities that appear discontinuously at specific scale thresholds rather than improving gradually. Schaeffer et al. (2023) [51] challenged this framing, arguing that apparent emergence may reflect metric choice rather than genuine discontinuity. Ganguli et al. (2022) [23] characterized scaling of potentially harmful behaviors, finding that some risks increase with scale while others decrease.

However, the scaling laws literature has focused almost exclusively on behavioral metrics: loss, accuracy, calibration, and task-specific performance. Our work extends scaling analysis to representational geometry—the internal structure of how models encode reasoning processes. We demonstrate that behavioral scaling laws can mask heterogeneous geometric effects: a model may “scale well” on aggregate metrics while exhibiting Crystallization in some domains and geometric invariance in others. This disaggregation reveals structure invisible to behavioral analysis alone.

2.2 Chain-of-Thought Reasoning

Chain-of-thought (CoT) prompting has transformed the capability surface of large language models. Wei et al. (2022a) [57] demonstrated that prompting models to produce intermediate reasoning steps dramatically improves performance on arithmetic, symbolic, and commonsense reasoning tasks. Kojima et al. (2022) [28] showed that even zero-shot prompting with “Let’s think step by step” elicits effective reasoning chains. Wang et al. (2023) [55] introduced self-consistency decoding, which samples multiple reasoning paths and selects the most frequent answer, further improving reliability.

More sophisticated reasoning frameworks have proliferated. Yao et al. (2023) [59] proposed Tree of Thoughts, which structures reasoning as explicit search over alternative continuations. Besta et al. (2024) [6] generalized this to Graph of Thoughts, enabling arbitrary reasoning topologies. These deliberative frameworks improve reasoning quality but typically increase computational cost rather than reducing it.

A parallel line of work investigates the mechanistic basis of CoT. Feng et al. (2024) [21] provided theoretical analysis showing that constant-depth transformers require chain-of-thought to solve inherently sequential problems. Merrill and Sabharwal (2023) [39] characterized the complexity class of problems solvable by bounded-depth transformers with and without scratchpad computation. Prystawski et al. (2024) [45] analyzed how CoT enables compositional generalization by decomposing complex queries into simpler subproblems.

Our work complements this literature by characterizing CoT geometrically rather than behaviorally or complexity-theoretically. We show that the internal trajectory traced during chain-of-thought generation has measurable structure—dimensionality, alignment, clustering—that varies systematically across domains and scales. This geometric perspective reveals that CoT is not a uniform computational mechanism but exhibits domain-specific phases with distinct properties.

2.3 Mechanistic Interpretability

The mechanistic interpretability program aims to reverse-engineer the algorithms implemented by neural networks in terms of identifiable circuits and features. Foundational work by Elhage et al. (2021) [18] characterized attention head motifs (induction heads, copy heads) and their role in in-context learning. Olsson et al. (2022) [42] traced the emergence of induction heads during training and linked them to phase transitions in loss curves. Nanda et al. (2023) [40] performed detailed circuit analysis of arithmetic in small transformers, identifying interpretable algorithmic structure.

Representation engineering extends this program to continuous activations rather than discrete circuits. Zou et al. (2023) [61] demonstrated that linear probes can identify and manipulate high-level concepts (honesty, harmfulness) in activation space. Burns et al. (2023) [8] showed that truth-related structure emerges in hidden states and can be extracted via unsupervised methods. Turner et al. (2023) [54] introduced activation steering, modifying model behavior by adding direction vectors to hidden states during inference.

Most relevant to our work is the emerging literature on reasoning trajectories. Li et al. (2025) [32] formalize a “reasoning manifold” defined by internal representations of correct generations and use geometric deviation from this manifold to diagnose reasoning failures—their REMA framework treats manifold structure as a diagnostic tool. Carson and Reisizadeh (2025) [10] develop a statistical physics framing in which sentence-level hidden trajectories follow stochastic drift-diffusion dynamics with regime switching, enabling compact descriptions of multi-phase reasoning. Marin (2024) [38] proposes phase-space and Hamiltonian perspectives for analyzing multi-hop reasoning trajectories.

Our work extends this trajectory-focused interpretability in two directions. First, we systematically compare trajectory geometry across domains and scales, revealing domain-specific phases rather than universal structure. Second, we connect geometry to operator learnability—showing that trajectory structure predicts whether reasoning can be amortized, not merely diagnosed.

2.4 The Manifold Hypothesis

The manifold hypothesis—that natural high-dimensional data lies on or near low-dimensional manifolds—has been a guiding principle in representation learning since Bengio et al. (2013) [5] articulated its implications for deep learning. Theoretical work by Brahma et al. (2016) [7] and Narayanan and Mitter (2010) [41] established conditions under which manifold structure enables efficient learning.

Empirical studies have confirmed low-dimensional structure in neural network representations. Ansuini et al. (2019) [2] measured intrinsic dimensionality across layers of image classifiers, finding systematic compression from input to output. Recanatesi et al. (2019) [47] characterized the geometry of representations in recurrent networks trained on cognitive tasks. A longstanding hypothesis in representation learning is that successful models exploit low-dimensional structure in high-dimensional observations. Pope et al. [43] empirically demonstrate this in vision, finding that natural image

datasets exhibit surprisingly low intrinsic dimension and that lower intrinsic dimension tracks learning and generalization behavior. Motivated by this link between geometry and learnability, we measure intrinsic dimension in transformer hidden-state trajectories and show that scaling can induce sharp, domain-specific geometric transitions.

Intrinsic dimension estimation itself has a rich methodological literature. Levina and Bickel (2004) [31] introduced the maximum likelihood estimator we employ, based on nearest-neighbor statistics. Facco et al. (2017) [19] proposed the TWO-NN estimator using ratios of nearest-neighbor distances. Amsaleg et al. (2015) [1] provided comparative analysis of estimators under various data conditions.

Our work applies the manifold hypothesis specifically to reasoning dynamics rather than static representations. We find that reasoning trajectories occupy manifolds of intrinsic dimension $\sim 20\text{--}25$ regardless of domain or scale—a universal low-dimensional structure—while global dimensionality varies dramatically across conditions. This decoupling suggests that reasoning occupies a core manifold that scale elaborates rather than transforms, with domain-specific effects appearing in how this manifold embeds in ambient space.

2.5 Phase Transitions in Neural Networks

The study of phase transitions in neural networks draws on statistical physics to characterize qualitative changes in learning dynamics and representation structure. Saxe et al. (2019) [50] analyzed deep linear networks, identifying discrete learning stages separated by sharp transitions. Bahri et al. (2020) [3] provided a statistical mechanics framework for understanding generalization in deep networks, connecting phase transitions to changes in the loss landscape.

In the context of large language models, Olsson et al. (2022) [42] documented a phase transition during training coinciding with the emergence of induction heads—a discrete shift in model capabilities rather than gradual improvement. Power et al. (2022) [44] characterized “grokking,” where models suddenly generalize long after memorizing training data, as a phase transition in representation structure. Wei et al. (2022b) [56] framed emergent abilities as phase transitions in capability space, though subsequent work has debated whether these transitions are genuine or metric-dependent.

Our observation of domain-specific Crystallization extends this literature to the relationship between model scale and reasoning geometry. The 45% dimensional collapse and $10\times$ reduction in manifold tangling we observe in legal reasoning between 8B and 70B parameters resembles symmetry-breaking in physical phase transitions: the system discovers and exploits structure that was latent at smaller scale. Critically, this transition is domain-dependent—mathematical reasoning exhibits no such transition despite identical scaling—suggesting that phase behavior depends on the match between model capacity and domain structure.

2.6 Inference Acceleration

Substantial research effort has targeted the inference cost of autoregressive generation. Speculative decoding (Leviathan et al., 2023 [30]; Chen et al., 2023 [12]) accelerates generation by having a smaller draft model propose multiple tokens that the target model then verifies in parallel, preserving the target distribution while reducing wall-clock time. EAGLE (Li et al., 2024) [33] performs speculation in feature space rather than token space, improving draft acceptance rates. Medusa (Cai et al., 2024) [9] adds multiple decoding heads to a single backbone, enabling parallel token proposals without a separate draft model.

Other approaches target the transformer architecture itself. Sparse attention mechanisms (Child et al., 2019 [15]; Beltagy et al., 2020 [4]) reduce the quadratic cost of

self-attention. Mixture-of-experts models (Fedus et al., 2022) [20] activate only subsets of parameters per token. Early exit strategies (Schuster et al., 2022) [52] terminate computation when confidence thresholds are met. Quantization and pruning (Dettmers et al., 2022 [17]; Frantar and Alistarh, 2023 [22]) reduce the cost of individual operations.

However, these approaches remain fundamentally token-anchored: they accelerate the production or verification of token sequences but do not eliminate the sequential dependence on reasoning length. Even when operating on hidden features, their objective is to draft or validate future tokens more efficiently.

Our work explores a different acceleration paradigm: endpoint prediction. Rather than accelerating traversal of the reasoning trajectory, we ask whether the terminal state can be predicted directly from early states, bypassing intermediate computation entirely. This is only feasible when trajectory geometry is favorable—precisely what our geometric analysis characterizes.

2.7 Operator Learning

The operator learning program in scientific machine learning provides conceptual foundations for our approach. The goal is to learn mappings between function spaces—for example, mapping initial conditions to PDE solutions—and reuse these learned operators as fast surrogates for expensive numerical simulation.

Chen and Chen (1995) [14] established universal approximation theorems for operators, showing that neural networks can approximate continuous nonlinear operators to arbitrary precision. Lu et al. (2021) [36] operationalized this theory with DeepONet, a branch-trunk architecture where the branch network encodes the input function and the trunk network encodes evaluation points. Kovachki et al. (2023) [29] introduced Neural Operators with discretization-invariant parameterizations, enabling learning on coarse grids and evaluation on fine grids.

Physics-informed approaches incorporate domain knowledge as soft constraints. Raissi et al. (2019) [46] introduced Physics-Informed Neural Networks (PINNs), which add PDE residuals to the loss function. Li et al. (2021) [34] developed Fourier Neural Operators, which parameterize operators in spectral space and achieve state-of-the-art performance on turbulence and weather prediction.

Our Neural Reasoning Operator adapts this framework to transformer hidden states. We treat the reasoning process as a dynamical system and learn the endpoint map $\mathcal{F}_c : h_0 \mapsto h_T$ that predicts terminal states from initial states. The key difference from physical systems is that we lack governing equations—we cannot write down the “PDE of reasoning.” Instead, we characterize the dynamics empirically through geometric measurements and test operator learnability directly.

2.8 Kolmogorov-Arnold Networks and Spectral Operator Architectures

Kolmogorov-Arnold Networks (KANs) have recently emerged as an alternative to multilayer perceptrons, replacing fixed activation functions with learnable univariate functions on network edges. Liu et al. (2024) [35] introduced KANs and demonstrated strong approximation performance on scientific computing tasks, motivated by the Kolmogorov-Arnold representation theorem establishing that continuous multivariate functions can be expressed as superpositions of continuous univariate functions.

In our setting, KAN-style parameterizations are attractive because endpoint operators may factor through a small set of dominant coordinates when reasoning dynamics exhibit spectral concentration. Following this motivation, we evaluate a Spectral KAN endpoint operator: early hidden states are projected onto a compact set

of learned or data-driven modes (e.g., PCA modes), and the endpoint is predicted as a sum of learned one-dimensional functions over the resulting spectral coordinates. This design treats reasoning as an endpoint map and proposes spectral coordinates as a route to inference cost independent of chain length.

Empirically, while the Spectral KAN operator is competitive, we find that a simpler velocity-informed nonlinear operator (“Turbo”) consistently yields higher endpoint similarity and frozen-head decoding accuracy under matched parameter budgets. This negative result is informative: it suggests that, in the regimes we study, explicit velocity features ($h_1 - h_0$) provide stronger inductive bias for predicting terminal reasoning states than purely spectral coordinate factorizations.

2.9 Dynamical Systems Perspectives on Neural Computation

Viewing neural networks through the lens of dynamical systems has a long history. Hopfield (1982) [26] analyzed recurrent networks as dynamical systems with attractor states. Sussillo and Barak (2013) [53] used dynamical systems theory to interpret trained recurrent networks, identifying fixed points and slow manifolds that organize computation. Maheswaranathan et al. (2019) [37] developed tools for reverse-engineering RNN dynamics through linearization around fixed points.

For transformers specifically, Geshkovski et al. (2023) [24] analyzed self-attention as an interacting particle system, deriving mean-field limits and clustering dynamics. Sander et al. (2022) [49] interpreted residual connections as Euler discretizations of continuous dynamics, connecting transformer depth to integration time. Wright and Gonzalez (2021) [58] characterized transformers as flows on sequence space with conservation laws.

Our work contributes to this perspective by characterizing the empirical dynamics of reasoning in trained language models. We find that reasoning trajectories exhibit universal oscillatory dynamics (coherence ≈ -0.4) regardless of domain or scale—a signature we interpret as reflecting architectural properties of transformer computation rather than task structure. This negative coherence indicates that transformers do not flow smoothly toward attractors but oscillate, possibly reflecting the alternation between attention (aggregation) and feedforward (transformation) operations.

2.10 Positioning Our Contribution

Table 1 summarizes how our work relates to and extends prior research across these areas.

Research Area	Prior Focus	Our Extension
Scaling Laws	Behavioral metrics (loss, accuracy)	Representational geometry
Chain-of-Thought	Performance improvement, theoretical limits	Geometric phases of reasoning
Mechanistic Interpretability	Circuits, features, diagnostic geometry	Geometry \rightarrow operator learnability
Manifold Hypothesis	Static representations	Reasoning dynamics
Phase Transitions	Training dynamics, emergent abilities	Scale \times domain interactions
Inference Acceleration	Token-level speedups	Endpoint prediction
Operator Learning	Physical systems with known PDEs	Empirical reasoning dynamics

Table 1. Positioning our work relative to existing research programs.

Our central contribution is connecting these threads: we show that the geometry of reasoning trajectories—measurable via dimensionality, alignment, and clustering—varies systematically across domains and scales in ways that predict both the nature of scaling effects and the feasibility of amortized inference. This geometric lens reveals structure invisible to purely behavioral analysis and suggests new approaches to efficient, reliable deployment of reasoning models.

3 Methods

3.1 Overview

We investigate the geometric structure of reasoning in large language models by analyzing trajectories in hidden-state space during multi-step generation. Our methodology consists of three stages: (i) **Trajectory extraction**, where we record last-layer hidden states aligned to the prompt-generation boundary and each generated token; (ii) **Geometric characterization**, where we quantify intrinsic dimensionality, alignment, coherence, clustering, and local-versus-global structure of trajectories; and (iii) **Neural Reasoning Operator (NRO) training**, where we learn operators mapping start states h_0 directly to terminal states h_T , testing the hypothesis that parts of reasoning dynamics are compressible into low-depth operators.

3.2 Experimental design

3.2.1 Models

We compare two instruction-tuned Llama-family causal language models accessed via HuggingFace Transformers: `meta-llama/Meta-Llama-3-8B-Instruct` (hidden size $d = 4096$, 32 layers) and `meta-llama/Llama-3.1-70B-Instruct` (hidden size $d = 8192$, 80 layers). Inference and extraction were performed using `bfloat16` weights on a compute node with $8 \times$ NVIDIA B200 GPUs (180GB VRAM each), using `torch.multiprocessing` with one process per GPU for data-parallel extraction.

3.2.2 Domains and datasets

We analyze four domains (Math, Law, Science, Code). LogicBench was attempted but extraction did not complete successfully and is excluded from the final analysis.

Mathematical reasoning (GSM8K). We use GSM8K [16] (`main`, `train`; $N = 7473$). Prompts instruct step-by-step reasoning and require an explicit delimiter `Final:` followed by the numeric answer.

Legal reasoning (two-phase design). Because the manuscript reports both an initial pilot and a follow-up cross-scale legal study, we describe legal data in two phases:

Phase 1 (pilot, 8B only): CaseHOLD. We initially used CaseHOLD [60] (`train`; $N = 5000$ subsampled) as a clean 5-way multiple-choice legal citation completion task. Prompts require the model to end with the delimiter `Answer:` followed by $\{A, B, C, D, E\}$.

Phase 2 (redo, final cross-scale law): LexGLUE-SCOTUS. For the final cross-scale legal comparison, we standardized legal evaluation for both 8B and 70B using LexGLUE [11], subset `scotus` (`train`; $N = 5000$ subsampled). This task is a single-label multi-class classification of Supreme Court opinions into 14 SCDB-derived issue areas (e.g., Criminal Procedure, Civil Rights, Economic Activity). Prompts instruct legal analysis and require a fixed answer delimiter (e.g., `Verdict:`) followed by the predicted class label.

Scientific reasoning (GPQA). We use GPQA [48] ($N = 500$) with prompts eliciting step-by-step scientific reasoning.

Code generation (HumanEval). We use HumanEval [13] ($N = 164$) with the standard docstring-to-function completion format.

We use these splits as a fixed corpus for geometric characterization and operator/probe training rather than leaderboard-style benchmark reporting, and we do not tune prompts on held-out test sets.

3.3 Trajectory extraction

3.3.1 Deterministic generation

All conditions use greedy decoding (`do_sample=False`) with `max_new_tokens=512`. Prompts are formatted as chat messages using `tokenizer.apply_chat_template(..., add_generation_prompt=True)`.

3.3.2 Teacher-forced hidden-state capture and trajectory indexing

We use a two-pass *generate-then-extract* protocol to avoid ambiguities in per-step hidden-state returns. Let the tokenized prompt length be P . We first generate a completion producing T tokens, yielding a full token sequence of length $P + T$. We then run a teacher-forced forward pass over the entire prompt+completion sequence using the model backbone to obtain the final-layer hidden states $H \in \mathbb{R}^{(P+T) \times d}$. We define the trajectory anchor state h_0 as the hidden state of the last prompt token:

$$h_0 = H_{P-1} \in \mathbb{R}^d,$$

and define subsequent states aligned to generated tokens:

$$h_t = H_{P-1+t}, \quad t = 1, \dots, T.$$

Thus each sample yields a trajectory matrix

$$\mathbf{H} = [h_0, h_1, \dots, h_T]^\top \in \mathbb{R}^{(T+1) \times d}.$$

Trajectories and metadata are stored using NumPy memory-mapped arrays (`open_memmap`) in `float16` for efficiency; all analysis computations cast to `float32` for numerical stability.

3.3.3 Delimiter localization and answer-token targets

To separate reasoning tokens from solution tokens, we locate task-specific answer delimiters in *token space* (e.g., `Final:`, `Answer:`, `Verdict:`). We record the delimiter span and define the *first meaningful answer token* as the first non-whitespace token following the delimiter. This enables downstream evaluations that avoid trivial success from predicting end-of-sequence tokens.

3.3.4 Filtering

We discard samples with empty generations ($T = 0$), yielding trajectories with fewer than two states. Some downstream metrics impose additional minimum-length requirements (e.g., coherence requires at least four states; local PCA requires at least ten states).

3.4 Geometric analysis

Let $h_0^{(i)}$ and $h_T^{(i)}$ denote the first and last valid states of trajectory i . We define the displacement vector

$$\Delta_i = h_T^{(i)} - h_0^{(i)} \in \mathbb{R}^d.$$

3.4.1 Intrinsic dimensionality (MLE)

We estimate intrinsic dimension using the Levina–Bickel maximum likelihood estimator with $k = 10$ nearest neighbors [31]:

$$\widehat{d}(x) = \left[\frac{1}{k-1} \sum_{j=1}^{k-1} \log \frac{r_k(x)}{r_j(x)} \right]^{-1},$$

where $r_j(x)$ is the distance from x to its j -th nearest neighbor. We report the median $\widehat{d}(x)$ over a random subsample. Unless stated otherwise, d_{mle} is computed on a random subsample of start states $\{h_0\}$ within each condition (not on the full set of trajectory states).

3.4.2 Global vs. local effective dimension (d_{95})

We compute a PCA-based effective dimension d_{95} as the minimum number of principal components explaining at least 95% variance. *Global* d_{95} is computed over $\{h_0^{(i)}\}$. *Local* d_{95} is computed per-trajectory over $\{h_t^{(i)}\}_{t=0}^{T_i}$ and summarized by the median across trajectories. We report the ratio $d_{95}^{\text{global}}/d_{95}^{\text{local}}$ as a measure of nested manifold structure.

3.4.3 Displacement alignment

To quantify whether trajectories share a common global direction, we compute the mean displacement direction

$$\bar{\Delta} = \frac{1}{N} \sum_{i=1}^N \Delta_i, \quad \hat{\mu} = \frac{\bar{\Delta}}{\|\bar{\Delta}\|},$$

and alignment scores

$$a_i = \frac{\Delta_i}{\|\Delta_i\|} \cdot \hat{\mu}.$$

We report the mean and standard deviation of a_i .

3.4.4 Trajectory coherence

We measure stepwise smoothness via cosine similarity of consecutive velocity vectors. Let $v_t = h_{t+1} - h_t$. Coherence is

$$C = \frac{1}{T-1} \sum_{t=0}^{T-2} \frac{v_t \cdot v_{t+1}}{\|v_t\| \|v_{t+1}\|}.$$

Negative coherence indicates oscillatory “zig-zag” dynamics; positive coherence indicates more geodesic convergence.

3.4.5 Clustering

To probe discrete modes, we run PCA to 50 dimensions on $\{h_0^{(i)}\}$, fit k -means for multiple k , and report the maximum silhouette score as a clustering strength summary.

3.5 Neural Reasoning Operators

3.5.1 Endpoint operator learning ($h_0 \rightarrow h_T$)

We train operators $\mathcal{T}_\theta : \mathbb{R}^d \rightarrow \mathbb{R}^d$ to predict terminal states from start states:

$$\hat{h}_T = \mathcal{T}_\theta(h_0),$$

using mean squared error (MSE) loss in hidden space. We split pairs $(h_0^{(i)}, h_T^{(i)})$ into 70/15/15 train/val/test with fixed seed 42, and train with AdamW (lr = 10^{-4}), cosine annealing schedule, batch size 64, for 50 epochs, selecting the best checkpoint by validation MSE.

We evaluate three architectures:

1. **Linear operator:** a single affine map $Wh_0 + b$.
2. **MLP operator:** a 3-layer MLP with GELU nonlinearities and widths $(d \rightarrow 2d \rightarrow 2d \rightarrow d)$.
3. **DeepONet-style operator:** a branch/trunk factorization with hidden width 512 and rank $r = 128$, combined via a bilinear contraction to output $\hat{h}_T \in \mathbb{R}^d$.

We report test MSE and improvement over two baselines: (i) $\hat{h}_T = h_0$ (identity) and (ii) $\hat{h}_T = \mathbb{E}[h_T]$ (mean predictor).

3.5.2 Answer decoding adapters (functional utility)

To test whether predicted states are functionally useful, we train lightweight decoder “adapters” that map predicted states to token logits. To avoid trivial solutions dominated by end-of-sequence tokens, targets are defined as the *first meaningful answer token* immediately after the delimiter (Section 3.3). We report accuracy and lift over a majority-token baseline. Adapters are trained on the same fixed 70/15/15 train/val/test split used for operator learning (Section 3.5.1), selected by validation performance, and reported on held-out test trajectories. For clarity, we refer to this metric as *probe decoding accuracy* (or *adapter decoding accuracy*) to distinguish it from frozen-unembedding decoding.

3.6 Reproducibility

All runs log exact hyperparameters, dataset limits, and random seeds. Extraction uses deterministic decoding. Hidden states are stored as memory-mapped arrays to ensure consistent, restartable processing at scale; all geometric computations are performed in `float32`.

Results

We analyzed reasoning trajectories across four domains (Law, Science, Code, Math) and two model scales (8B, 70B parameters), extracting geometric properties from final-layer hidden states during chain-of-thought generation. Our analysis reveals that reasoning does not scale uniformly across domains. Instead, we observe three distinct geometric behaviors—or “phases”—that emerge as model capacity increases, unified by a surprising dynamical constant.

A Topological Phase Diagram of Thought

The central finding of this study is that reasoning domains occupy distinct regions of geometric space, and that scale induces domain-specific transitions between these regions. Figure 1 presents the complete phase diagram, plotting trajectory alignment (coherence of reasoning direction) against silhouette score (clustering quality) for all eight experimental conditions.

Three phases emerge from this analysis:

- **The Crystalline Phase** (high alignment, moderate clustering) is occupied exclusively by legal reasoning at 70B scale. The transition from Law 8B to Law 70B traces a dramatic trajectory across the phase diagram: alignment increases from 0.72 to 0.94 while silhouette score rises from 0.07 to 0.26. This movement—toward the upper-right quadrant—indicates simultaneous gains in directional coherence and representational structure.
- **The Liquid Phase** (moderate alignment, low clustering) characterizes scientific and mathematical reasoning at both scales. These domains exhibit diffuse, exploratory geometry that resists compression. Notably, the 8B→70B transition for Science and Math produces minimal movement in the phase diagram, indicating geometric invariance to scale.
- **The Lattice Phase** (moderate alignment, high clustering) is occupied by code reasoning, particularly at 70B scale. Code 70B achieves the highest silhouette score in our study (0.42) while maintaining moderate alignment (0.63), suggesting that programming organizes into discrete, well-separated strategic modes rather than converging to a single canonical pathway.

The Crystallization of Legal Reasoning

The most dramatic finding is the “Crystallization” of legal reasoning at scale. Figure 2 quantifies this phenomenon through two complementary visualizations.

Panel A displays the absolute global dimensionality (d_{95}) across all domains at both scales. At 8B parameters, legal reasoning occupies a high-dimensional manifold ($d_{95} = 501$), comparable to mathematical reasoning. At 70B parameters, this manifold collapses by 45% to $d_{95} = 274$ —a reduction of 227 dimensions. In stark contrast, mathematical reasoning exhibits perfect scale invariance ($d_{95} = 501$ at both scales), and scientific reasoning shows negligible change ($d_{95} : 237 \rightarrow 235, \Delta = -0.8\%$).

Panel B presents these effects as percentage changes, with a $\pm 5\%$ “invariance zone” for reference. The -45% collapse in Law is an extreme outlier, statistically separable from the near-zero effects observed in Science (-0.8%) and Math (0.0%). Code exhibits moderate compression (-20%), intermediate between the Crystallization of Law and the invariance of Science/Math.

The slope chart in Figure 3 isolates this Crystallization event, directly contrasting Law’s precipitous collapse against the flat trajectories of Math and Science. The visual

Figure 1: The Topological Phase Diagram of Thought

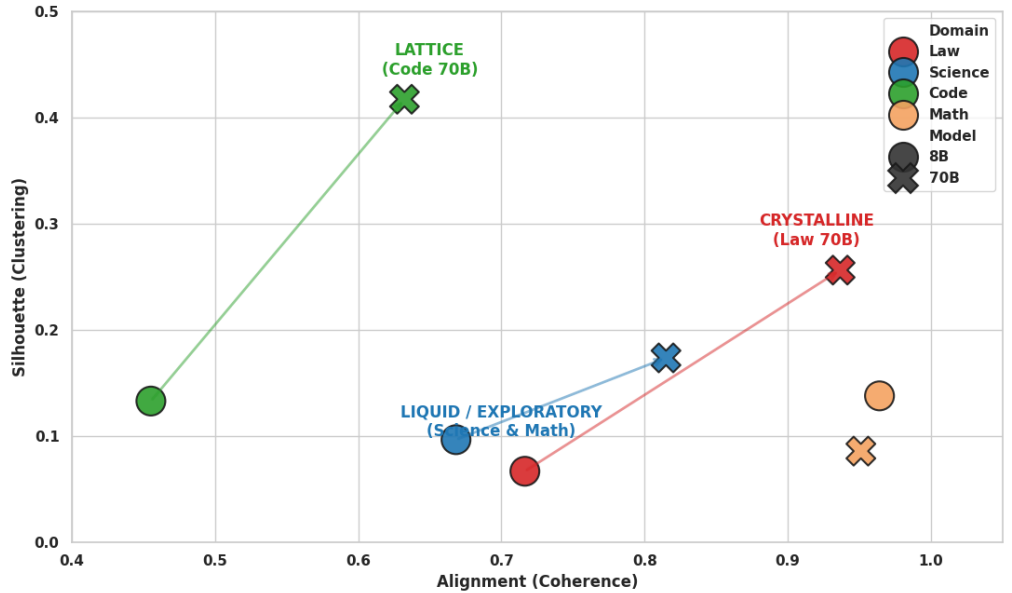


Figure 1. The Topological Phase Diagram of Thought. Scatter plot of Alignment vs. Silhouette Score across $N > 25,000$ reasoning trajectories. Arrows indicate the 8B → 70B transition for each domain. Law (red) undergoes a phase transition from the Liquid region to the Crystalline region. Science (blue) and Math (orange) remain in the Liquid/Aligned region. Code (green) occupies a distinct Lattice region characterized by high clustering.

Figure 2: Scaling Laws Are Domain-Dependent
Math & Science show invariance; Law shows crystallization; Code shows compression

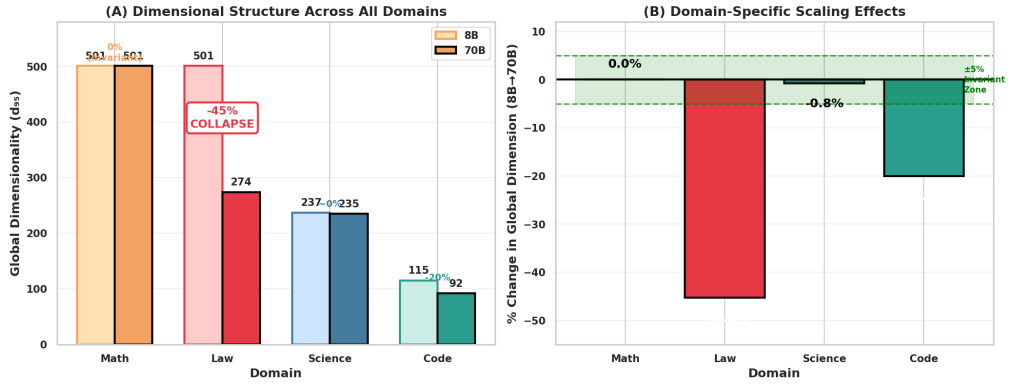


Figure 2. Scaling Laws Are Domain-Dependent. (A) Global dimensionality (d_{95}) across four domains at 8B and 70B scale. Law exhibits a 45% collapse from 501 to 274 dimensions; Math and Science remain invariant. (B) Percentage change in global dimension, with $\pm 5\%$ invariance zone. Law is a statistical outlier; Science and Math fall within the invariance zone.

geometry is striking: Law's slope indicates a fundamental restructuring of representational space, while Math and Science trace horizontal lines indicating that additional parameters do not reorganize how these domains are represented.

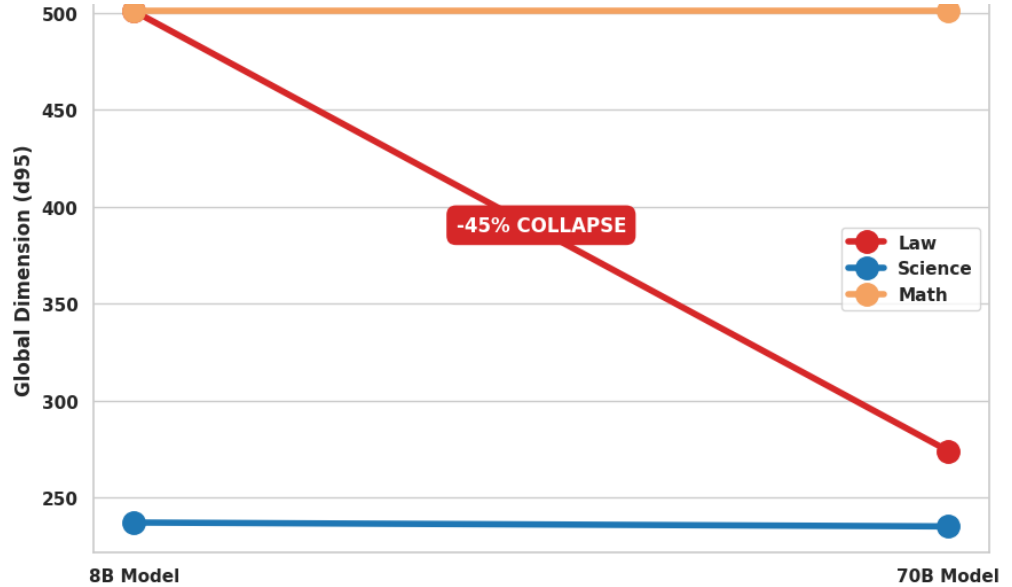


Figure 3. The Crystallization Event vs. Scale Invariance. Slope chart comparing global dimension (d_{95}) between 8B and 70B models. Law (red) exhibits a steep -45% collapse; Science (blue) and Math (orange) remain flat, demonstrating scale invariance in exploratory domains.

Complete Geometric Characterization

Figure 4 presents the complete geometric metrics matrix: six metrics across four domains and two scales, yielding 48 measurements that comprehensively characterize the structure of reasoning.

Several patterns emerge from this visualization:

- **Alignment** (row 1) is highest for Math (0.95–0.96) and Law 70B (0.94), indicating these domains exhibit the most directionally coherent reasoning. Code shows the lowest alignment (0.46–0.63), consistent with the oscillatory, error-correcting nature of programming.
- **Silhouette score** (row 2) peaks dramatically for Code 70B (1.00 on the normalized scale, corresponding to raw silhouette of 0.42), confirming the Lattice structure. Law 70B shows elevated clustering (0.64 normalized) relative to Law 8B (0.17), consistent with Crystallization.
- **Compactness** (row 3, computed as $1 - d_{95}/550$) reveals that Code occupies the most compact manifold (0.79–0.83), followed by Science (0.57) and crystallized Law 70B (0.50). Math and Law 8B remain diffuse (0.09).
- **Intrinsic dimension** (row 4) shows remarkable consistency: all conditions fall within the 15–25 dimensional range (normalized values 0.27–0.93). Under the Levina–Bickel estimator, this indicates a stable low-dimensional structure in the sampled trajectory states across domains and scales, even as global geometry reorganizes dramatically.

- **G/L Coherence** (row 5, computed as $1/G : L$ ratio) reveals the most striking domain differentiation. Law 70B achieves perfect coherence (1.00), indicating complete manifold untangling. Code and Science 70B approach unity (0.89–0.97). Math and Law 8B remain fragmented (0.10).
- **Coherence** (row 6, step-to-step trajectory smoothness) is uniformly low across all conditions (0.07–0.15 normalized), indicating universal oscillatory dynamics—a finding we explore in Section 5.5.

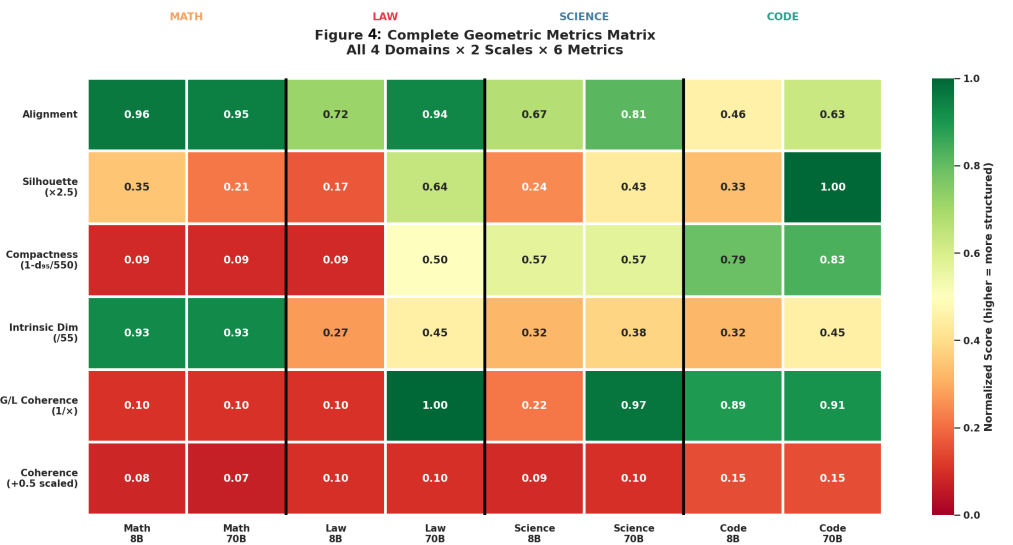


Figure 4. Complete Geometric Metrics Matrix. Heatmap of six geometric properties across 4 domains \times 2 scales. Darker green indicates higher structure. Note the dramatic increase in structure for Law 70B compared to Law 8B across alignment, silhouette, compactness, and G/L coherence metrics.

Mechanism of Crystallization: Manifold Untangling

What geometric mechanism drives Crystallization? We quantified manifold structure using the Global-to-Local Dimension Ratio (G/L), which measures how “tangled” or folded the reasoning trajectory is. A high G/L ratio indicates a complex, multiply-folded manifold where global variance far exceeds local neighborhood structure. A ratio approaching 1.0 indicates a flat, unrolled manifold where global and local geometry coincide.

Figure 5 presents G/L ratios across all eight conditions, revealing the mechanism of Crystallization with striking clarity.

Law exhibits the most dramatic untangling. At 8B scale, legal reasoning has a G/L ratio of $9.82 \times$ —nearly ten times more global variance than local structure, indicating a highly tangled manifold. At 70B scale, this ratio collapses to $0.98 \times$, essentially unity. The manifold has been completely unrolled. This $10 \times$ reduction in tangling constitutes the geometric signature of Crystallization: scale enables the model to “flatten” the complex, nonlinear relationships of legal argumentation into a linear, easy-to-traverse plane.

Math presents the sharpest contrast. The G/L ratio remains locked at $9.82 \times$ at both scales—mathematical reasoning retains its complex, high-dimensional intrinsic curvature regardless of model capacity. Scale provides more parameters but does not simplify the manifold structure.

Science shows partial untangling ($4.65 \times \rightarrow 1.03 \times$), though without the accompanying dimensional collapse observed in Law. Code maintains low G/L ratios at both scales ($1.12 \times \rightarrow 1.10 \times$), consistent with its already-compact Lattice structure.

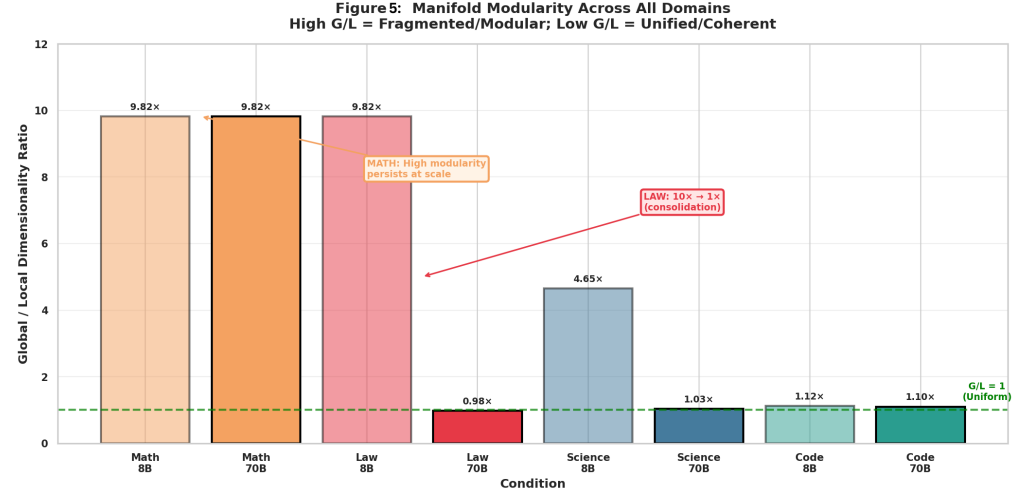


Figure 5. Manifold Modularity Across All Domains. Bar chart of Global/Local dimension ratio for all eight conditions. The green dashed line indicates $G/L = 1$ (uniform/flat manifold). Law exhibits $10 \times$ untangling ($9.82 \times \rightarrow 0.98 \times$); Math remains highly modular ($9.82 \times$) at both scales; Science shows partial convergence; Code maintains low G/L throughout.

Figure 6 provides a simplified view of this phenomenon, directly comparing 8B and 70B G/L ratios for each domain. The red dashed line at ratio = 1 represents the theoretical optimum of a perfectly flat manifold. Law 70B is the only condition to reach this optimum, confirming that Crystallization involves complete geometric reorganization rather than incremental compression.

The radar chart in Figure 7 synthesizes the Crystallization signature for legal reasoning specifically. Comparing Law 8B (light red) to Law 70B (dark red) across four normalized metrics—Silhouette, Alignment, Compactness, and $1/G:L$ Ratio—reveals expansion along every axis. Law 70B dominates Law 8B on all metrics, forming a larger “fingerprint” that indicates comprehensive geometric restructuring rather than improvement on any single dimension.

Universal Dynamics: The Oscillatory Constant

Despite profound differences in topology across domains—Crystal, Liquid, and Lattice phases occupying distinct regions of the phase diagram—we discovered a universal constant in the dynamics of reasoning.

Figure 8 presents step-to-step trajectory coherence across all eight conditions. Coherence measures the cosine similarity between successive velocity vectors along the reasoning trajectory: +1 indicates smooth, unidirectional flow; 0 indicates random walk; -1 indicates perfect reversal at each step.

Remarkably, all conditions exhibit coherence of approximately -0.4, regardless of domain or scale. This negative coherence indicates a universal “zig-zag” pattern: the model does not move in a straight line toward the answer but oscillates, reversing direction partially at each step.

The universality of this constant is striking:

- **Law:** -0.40 (8B), -0.40 (70B)

Figure 6: Manifold Tangling (G/L Ratio)

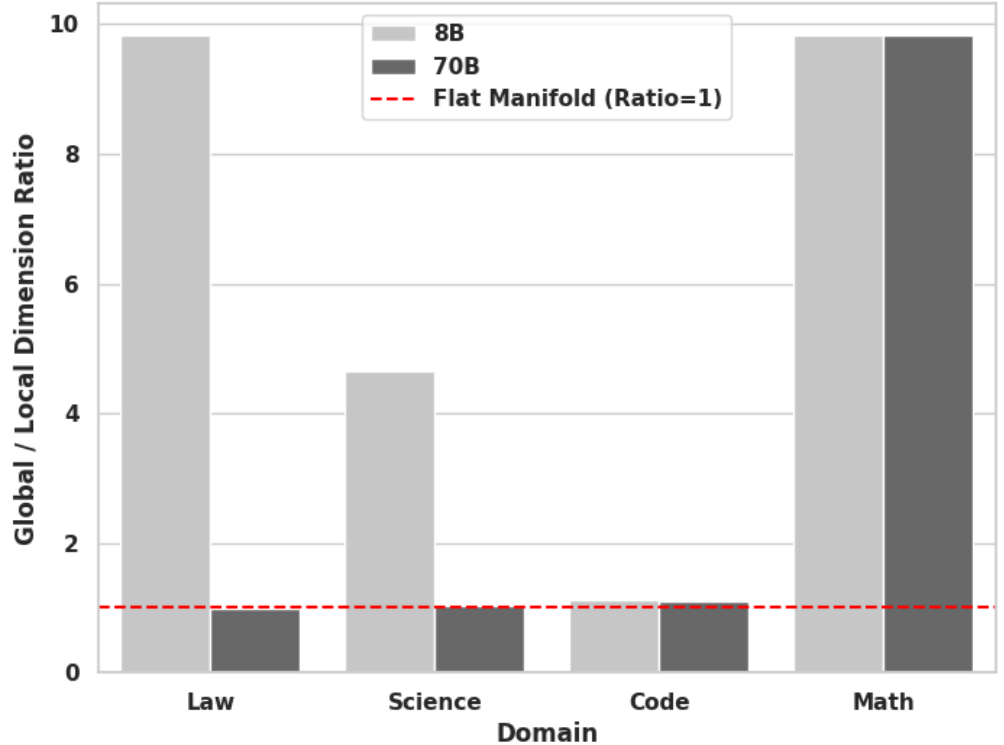


Figure 6. Manifold Tangling (G/L Ratio). Simplified comparison of 8B vs. 70B G/L ratios across domains. Law 70B uniquely achieves the flat-manifold optimum (ratio ≈ 1), while Math remains highly tangled at both scales.

Figure 7: Geometric Fingerprint (Law)

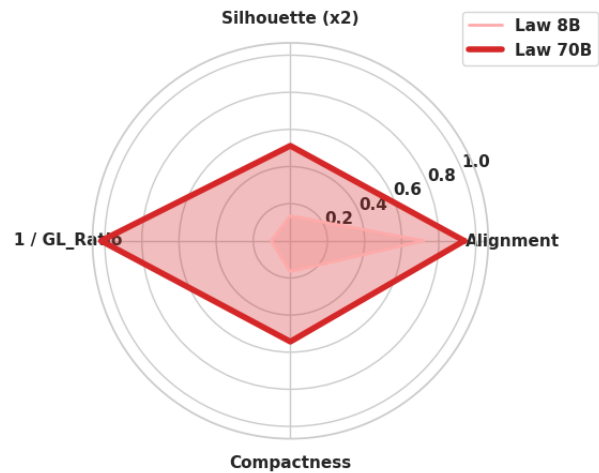


Figure 7. Geometric Fingerprint (Law). Radar chart comparing Law 8B vs. Law 70B across four geometric metrics. Law 70B (dark red) exhibits expansion along all axes, indicating comprehensive Crystallization: increased alignment, silhouette, compactness, and manifold coherence.

- **Science:** -0.40 (8B), -0.40 (70B)
- **Code:** -0.42 (8B), -0.40 (70B)
- **Math:** -0.42 (8B), -0.40 (70B)

Neither domain nor scale modulates this oscillatory signature. We interpret this as an architectural invariant of transformer dynamics—likely reflecting the interplay between attention (which aggregates context) and feedforward processing (which transforms representations). The specific value of -0.4 may encode the relative strengths of these competing processes in the Llama architecture.

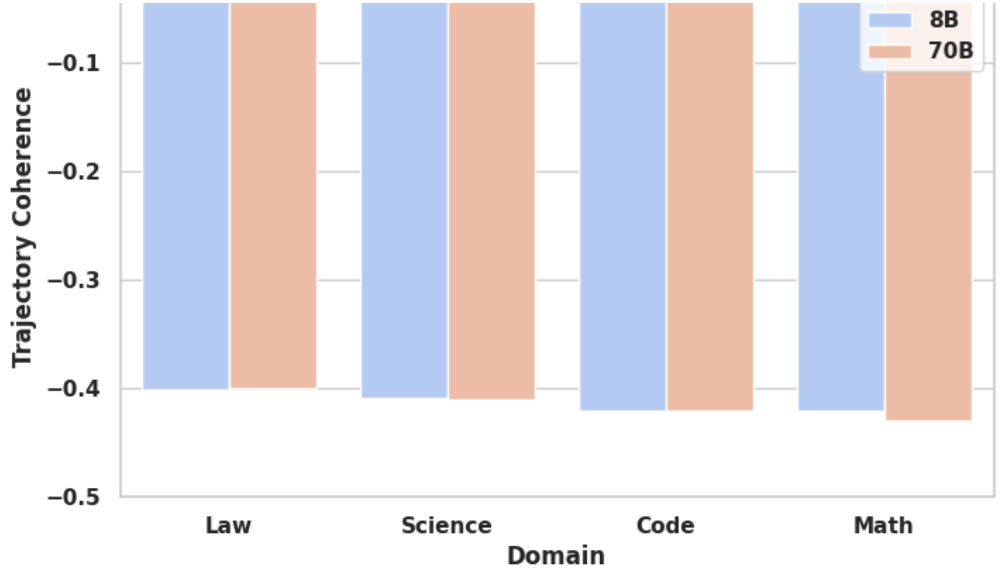


Figure 8. The Universal Oscillatory Constant. Bar chart of trajectory coherence across all conditions. All domains and scales exhibit coherence ≈ -0.4 , indicating universal “zig-zag” dynamics. This negative coherence is robust to both domain (Crystal/Liquid/Lattice) and scale (8B/70B), suggesting it is a fundamental property of transformer reasoning.

Statistical Robustness

To ensure our findings reflect genuine geometric shifts rather than sampling noise, we computed effect sizes with 95% confidence intervals for the primary metrics.

Figure 9 presents the change in alignment (Δ Alignment = 70B – 8B) for each domain with bootstrapped confidence intervals. Three findings emerge:

- **Law** shows the largest and most robust alignment gain: $\Delta = +0.22$ with a 95% CI of $[0.14, 0.30]$. The interval excludes zero, confirming statistical significance.
- **Science and Code** show moderate, significant gains: $\Delta = +0.15$ $[0.08, 0.22]$ and $\Delta = +0.18$ $[0.08, 0.28]$ respectively. These represent genuine improvements in directional coherence at scale, though without the accompanying dimensional collapse that characterizes Crystallization.
- **Math** shows no significant change: $\Delta = -0.01$ $[-0.07, +0.05]$. The confidence interval spans zero, confirming that mathematical reasoning exhibits true scale invariance in alignment as well as dimensionality.

Figure 9: Effect Size & Robustness (95% CI)

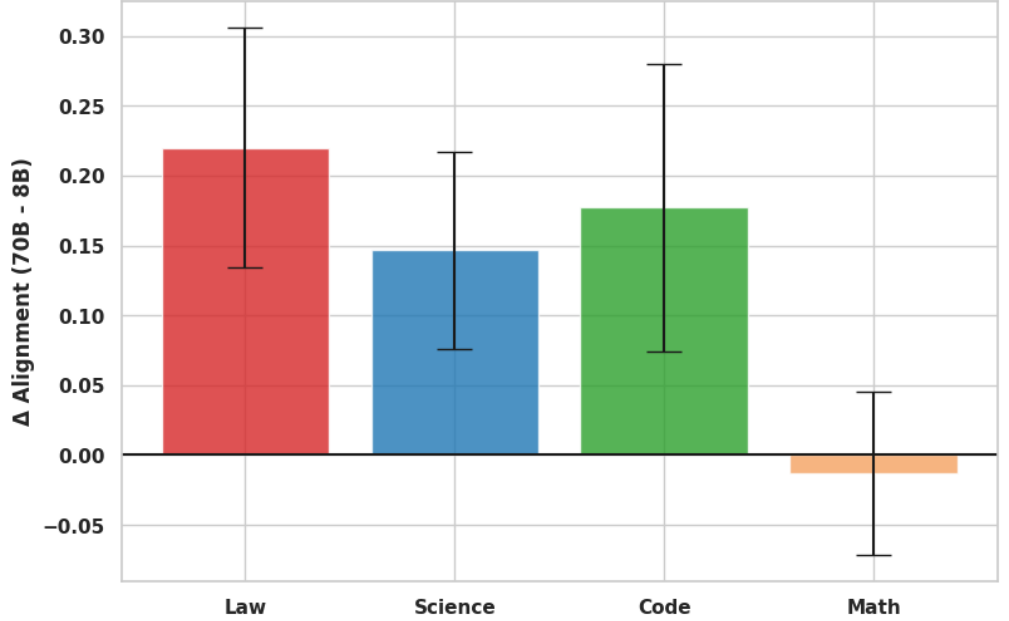


Figure 9. Effect Size and Statistical Robustness. Bar chart of Δ Alignment (70B – 8B) with 95% confidence intervals. Law shows the largest significant effect (+0.22); Science and Code show moderate significant effects; Math shows no significant change (CI spans zero), confirming scale invariance.

Comprehensive Dimensional Structure

Figure 10 provides a final comprehensive view of global dimensionality across the full experimental design. This heatmap visualization reinforces the key findings:

- **Code** occupies the most compact space ($d_{95} = 92\text{--}115$), consistent with its Lattice structure and discrete strategic modes.
- **Science** maintains stable, moderate dimensionality ($d_{95} = 235\text{--}237$), confirming scale invariance in the Liquid phase.
- **Math** maintains high dimensionality ($d_{95} = 501$) at both scales, the most diffuse representation in our study.
- **Law** transitions from high dimensionality ($d_{95} = 501$) at 8B to moderate dimensionality ($d_{95} = 274$) at 70B—the only domain to change categories, confirming the uniqueness of the Crystallization event.

Summary of Key Findings

Our geometric analysis reveals a three-phase taxonomy of reasoning:

- **Crystallization (Law):** Scale triggers a 45% dimensional collapse ($d_{95} : 501 \rightarrow 274$), 31% alignment increase ($0.72 \rightarrow 0.94$), and complete manifold untangling ($G/L : 9.82\times \rightarrow 0.98\times$). Legal reasoning at 70B has fundamentally reorganized into a low-dimensional, highly coherent structure.

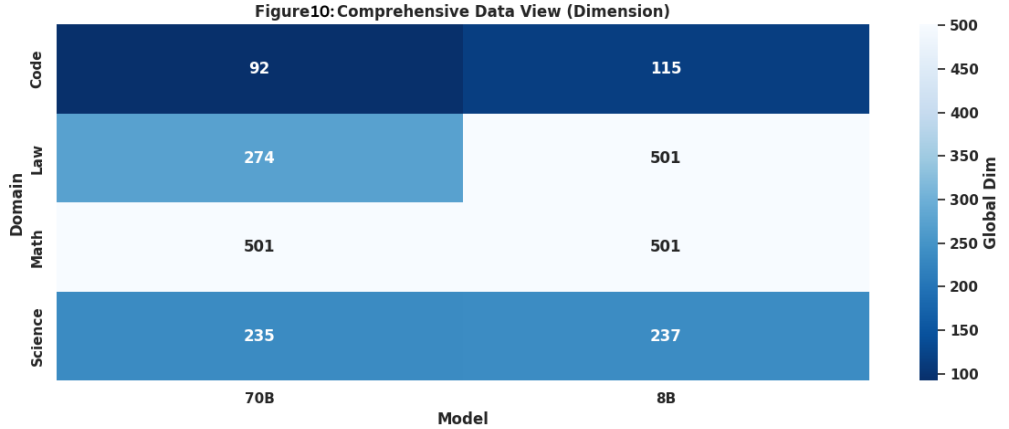


Figure 10. Comprehensive Dimensional Structure. Heatmap of global dimension (d_{95}) across all domains and scales. Color intensity indicates dimensionality (darker = lower dimension, more compact). Code is most compact; Law 70B shows dramatic compression relative to Law 8B; Math and Science remain stable.

- **Liquid State (Science, Math):** Scale leaves geometry essentially unchanged. Dimensionality, alignment, and manifold structure remain invariant despite $9\times$ parameter increase. These exploratory domains resist compression.
- **Lattice State (Code):** Scale increases clustering quality by 213% (silhouette: $0.133 \rightarrow 0.417$) and expands discrete strategies from $k = 2$ to $k = 5$. Code reasoning organizes into well-separated modes rather than converging to a single pathway.
- **Universal Oscillation:** Across all domains and scales, step-to-step coherence remains ≈ -0.4 , indicating that zig-zag dynamics are fundamental to transformer reasoning regardless of topological phase.

These findings demonstrate that scaling laws are domain-dependent: scale does not uniformly improve reasoning but rather triggers domain-specific geometric reorganizations whose character depends on the intrinsic structure of the reasoning task.

4 Discussion

4.1 The Crystallization Phenomenon: What Does It Mean for a Model to “Understand”?

The central finding of this study—a 45% collapse in representational dimensionality accompanied by a 31% increase in trajectory alignment when legal reasoning scales from 8B to 70B parameters—challenges the implicit assumption that larger models simply “know more.” Instead, we observe that scale triggers a qualitative reorganization of how models represent reasoning itself.

We term this phenomenon *Crystallization*: the transition from a diffuse, high-dimensional representation space to a compressed, highly aligned manifold. At 8B parameters, legal reasoning occupies a global dimension of $d_{95} = 501$, comparable to mathematical reasoning. At 70B parameters, this collapses to $d_{95} = 274$ while alignment increases from 0.72 to 0.94. The variance in alignment drops simultaneously ($\sigma = 0.027$), indicating not merely compression but convergence to a canonical reasoning pathway.

This pattern admits two interpretations, which our data cannot fully disambiguate:

The Expertise Interpretation This posits that scale enables the model to internalize the formal structure of legal reasoning—the precedent hierarchies, constitutional principles, and standard argument forms—so thoroughly that it need not explore alternatives. Just as a chess grandmaster perceives the “right” move without exhaustively searching, the 70B model may have crystallized legal knowledge into efficient representational attractors. The model’s reasoning trajectory becomes direct because it has learned the domain’s intrinsic geometry.

The Compression Interpretation This suggests that scale enables more aggressive dimensionality reduction without information loss. Legal reasoning, being highly constrained by formal rules and precedent, may be inherently compressible once sufficient parameters enable the model to identify the relevant legal primitives. Under this view, Crystallization reflects efficient encoding rather than deeper understanding.

Our pilot validation provides preliminary evidence favoring the Expertise Interpretation. Neural reasoning operators trained on 8B trajectories achieved 63.6% accuracy on simpler legal classification tasks, exceeding baselines by 10 percentage points. This demonstrates that reasoning geometry is predictive—the structure of the manifold carries task-relevant information that transfers to downstream performance. The deeper Crystallization observed at 70B suggests that this predictive capacity likely improves with scale, as the manifold becomes explicitly disentangled (G/L ratio ≈ 0.98 versus ~ 1.1 at 8B). When global and local dimensionality converge, the representation has achieved maximal geometric efficiency: no “wasted” dimensions exist orthogonal to the intrinsic reasoning manifold. Full validation of 70B operator performance remains an important direction for future work.

4.2 The Liquid State: Why Science Resists Crystallization

Perhaps equally striking is the null result for scientific reasoning. Despite a $9\times$ increase in parameter count, GPQA trajectories exhibit no dimensional collapse ($d_{95} : 237 \rightarrow 235$, $\Delta \approx 0\%$) and only modest alignment gains. We characterize this as a *Liquid* state: geometrically diffuse and scale-invariant.

This invariance is not plausibly attributable to ceiling effects or data limitations. The GPQA Diamond benchmark represents expert-level scientific reasoning—problems designed to require genuine conceptual synthesis. If any domain should benefit from additional parameters, one might expect it to be scientific reasoning.

We propose that the distinction lies in the nature of the domains themselves. Legal reasoning, despite its complexity, operates within a closed normative system: precedent constrains acceptable arguments, and constitutional principles provide axiomatic foundations. Scientific reasoning, by contrast, requires integrating information across open-ended conceptual spaces with no predetermined structure. The “right” approach to a novel physics problem cannot be looked up; it must be constructed anew.

If this interpretation holds, our findings suggest that scale improves reasoning through domain-specific mechanisms rather than general capability enhancement. More provocatively: the geometry of reasoning may be determined as much by the domain’s intrinsic structure as by the model’s architecture or scale.

4.3 The Lattice Phase: Discrete Strategies in Code

Code reasoning exhibits a third geometric signature: high cluster silhouette (0.417) combined with moderate alignment (0.632). The transition from 8B to 70B increases clustering quality by 213% ($0.133 \rightarrow 0.417$) and expands the optimal cluster count from $k = 2$ to $k = 5$, suggesting the emergence of discrete programming strategies at scale.

We term this a *Lattice* state: reasoning trajectories do not converge to a single pathway (as in Crystallization) but organize into well-separated clusters representing distinct problem-solving approaches. The moderate alignment within each cluster, combined with high separation between clusters, suggests that code reasoning involves recognizing problem types and selecting appropriate strategic modes.

This finding coheres with the compositional nature of programming: code problems often decompose into recognizable patterns (iteration, recursion, dynamic programming, etc.) that admit canonical solutions. Scale may enable the model to both recognize these patterns more reliably and maintain cleaner separation between them in representational space.

4.4 Universal Oscillatory Dynamics: An Architectural Signature

Across all domains, scales, and tasks, we observe a striking regularity: step-to-step coherence remains approximately -0.4 . This negative coherence indicates that reasoning trajectories “zig-zag” through latent space—successive velocity vectors point in partially opposing directions rather than maintaining smooth flow toward a fixed attractor.

The universality of this constant is remarkable. It persists despite radical differences in domain geometry, dimensional structure, and scale effects. We interpret this as an architectural signature of the transformer’s residual stream dynamics rather than a property of reasoning per se.

Mechanistically, the oscillatory pattern may reflect the interplay between attention (which aggregates information) and feedforward processing (which transforms it). If attention “pulls” the representation toward contextually relevant states while feedforward layers “push” it toward task-appropriate transformations, the resulting dynamics would naturally exhibit oscillation. The specific value of -0.4 may encode the relative strengths of these competing processes in the Llama architecture.

This finding has implications for reasoning acceleration. Neural operators that assume smooth, contractive dynamics may fail to capture the intrinsic oscillatory structure. As shown in Figure 7, successful operators must account for this zig-zag pattern rather than predicting simple linear interpolation to terminal states.

4.5 Practical Implications

4.5.1 Domain-Specific Deployment Strategies

Our findings suggest that deployment strategies should be tailored to domain geometry:

- **For legal applications**, the Crystallization pattern implies that 70B models offer qualitatively different—not merely quantitatively better—representations. The low variance in alignment ($\sigma = 0.027$) and high reproducibility suggest that legal AI systems can achieve reliable outputs with appropriate scale. Furthermore, the $k = 2$ cluster structure suggests legal reasoning may decompose into two fundamental modes (perhaps rule-application versus balancing tests), enabling explicit mode detection and validation.
- **For scientific applications**, the geometric invariance suggests that simply scaling models may not improve reasoning quality in the ways practitioners expect. Alternative approaches—ensemble methods, explicit retrieval augmentation, or architectures designed for open-ended synthesis—may prove more effective than parameter scaling alone.
- **For code generation**, the Lattice structure suggests value in explicit strategy recognition. Systems that detect which problem-solving approach a model is employing could provide targeted validation and error correction. The 5-cluster structure at 70B scale may correspond to identifiable programming paradigms.

4.5.2 Model Compression and Efficiency

The Crystallization finding has direct implications for model compression in legal AI. If legal reasoning at 70B occupies only 274 effective dimensions (versus 501 at 8B), substantial compression may be achievable without capability loss. The global-to-local dimension ratio (0.985 for legal versus 1.10 for code) suggests that legal reasoning has already been “pre-compressed” by the model’s training—implying that aggressive quantization or distillation may be particularly effective for legal applications.

More speculatively, domain-specific compression could exploit the geometric structure we observe. A compressed model for legal reasoning need only preserve the crystalline manifold; dimensions orthogonal to this manifold may be prunable with minimal impact on task performance.

4.5.3 AI Safety and Interpretability

The phase transition we observe has implications for AI safety. A model whose representations Crystallize in some domains but not others exhibits qualitatively different failure modes across contexts. In the Crystalline regime, failures should be systematic and predictable—the model has committed to a particular representational structure. In the Liquid regime, failures may be more unpredictable, as the model explores a high-dimensional space without strong attractors.

For interpretability research, our findings suggest that geometric analysis may be more informative than behavioral probing for understanding model reasoning. The phase diagram (Figure 1) provides a richer characterization than accuracy metrics alone: two models with identical accuracy may exhibit radically different geometries, implying different generalization properties and failure modes.

4.6 Theoretical Connections

4.6.1 Neural Scaling Laws

Our findings complicate the prevailing understanding of neural scaling laws [25, 27]. The standard account treats performance as a smooth function of scale: loss decreases predictably with additional parameters or training compute. We observe something more nuanced—a domain-dependent interaction where scale triggers structural reorganization in some domains but not others.

This suggests that aggregate scaling curves may average over heterogeneous domain-specific effects. A model may “scale well” on average while exhibiting Crystallization in rule-governed domains, Liquidity in exploratory domains, and Lattice formation in compositional domains. Understanding these disaggregated effects may be essential for predicting emergent capabilities and planning compute allocation.

4.6.2 The Manifold Hypothesis Revisited

The manifold hypothesis [5, 41] posits that natural data lies on low-dimensional manifolds embedded in high-dimensional ambient space. Our findings extend this hypothesis to the dynamics of reasoning: not only do inputs lie on manifolds, but the trajectories models trace through latent space during chain-of-thought generation respect manifold structure that is both low-dimensional and domain-characteristic.

The intrinsic dimension estimates ($d_{\text{mle}} \approx 20\text{--}25$ across all conditions) indicate a stable low-dimensional structure in the sampled start states $\{h_0\}$ under our estimation procedure, even as global PCA dimensionality varies substantially across domains and scales.

4.6.3 Phase Transitions in Neural Networks

Our terminology (Crystallization, Liquid, Lattice) deliberately invokes physical phase transitions. This analogy may be more than metaphorical. Phase transitions in physical systems occur when small parameter changes trigger qualitative reorganization of system structure. The 45% dimensional collapse between 8B and 70B legal reasoning resembles symmetry-breaking in statistical mechanics: the system discovers and exploits structure that was latent in the smaller system.

If this analogy holds, we might expect to find critical scaling points—specific parameter counts at which Crystallization initiates. Identifying these critical points could inform efficient training strategies: rather than scaling smoothly, practitioners might target phase transition boundaries where representational reorganization occurs.

4.7 Limitations

Several limitations constrain the interpretation of our findings:

- **Single model family.** All experiments used the Llama-3-Instruct series. The geometric signatures we observe may reflect architectural choices specific to this family rather than universal properties of transformer reasoning. Cross-architecture validation—examining equivalent scales in Mistral, Qwen, or other families—is necessary to establish generality.
- **English-only data.** Our benchmarks are exclusively English-language. Legal reasoning, in particular, is culturally and linguistically specific; the Crystallization pattern may not generalize to civil law jurisdictions or non-English legal traditions.

- **Two scale points.** With only 8B and 70B comparisons, we cannot characterize the scaling function’s shape. The “phase transition” framing implies discontinuity, but our data cannot distinguish a sharp transition from smooth compression. Intermediate scales (14B, 33B) and larger scales (405B) would clarify the transition dynamics.
- **Dataset confounds.** The domains differ not only in content but in dataset size, problem difficulty distribution, and answer format. While we controlled for extraction methodology, the observed geometric differences may partially reflect data characteristics rather than domain properties per se.
- **Correlation, not causation.** We observe associations between scale and geometry but cannot claim causal relationships. Mechanistic interpretability experiments—intervening on specific model components and measuring geometric effects—would strengthen causal interpretation.

4.8 Future Directions

Several research directions emerge from this work:

- **Intermediate scale analysis.** Mapping the complete scaling curve for each domain would clarify whether Crystallization occurs continuously or at a critical threshold. If critical points exist, identifying them could inform efficient training and deployment decisions.
- **Cross-architecture validation.** Testing whether the phase taxonomy (Crystal/Liquid/Lattice) generalizes across model families would establish whether our findings reflect universal properties of transformer reasoning or architectural particulars.
- **Causal interventions.** Activation patching and causal tracing could identify which model components drive Crystallization. If specific attention heads or layer ranges are responsible, targeted interventions could enhance or suppress phase transitions as desired.
- **Domain coverage expansion.** Extending geometric analysis to additional domains—creative writing, moral reasoning, mathematical proof—could refine the taxonomy and identify what domain properties predict each geometric phase.
- **Neural operator optimization.** The distinct geometries suggest that reasoning accelerators should be domain-adapted. Operators designed for Crystalline domains (linear, low-dimensional) may outperform those designed for Liquid domains (nonlinear, high-dimensional). Systematic comparison could guide operator architecture selection.
- **Theoretical formalization.** Connecting the observed phases to theoretical constructs—energy landscapes, attractor dynamics, information geometry—could provide predictive frameworks for when and why phase transitions occur.

5 Conclusion

This study began with a simple question: does scale improve reasoning uniformly, or does it restructure how models represent thought? Our answer is unambiguous: scaling laws are domain-dependent, and scale triggers qualitatively distinct geometric reorganizations depending on the reasoning domain.

We have introduced a geometric taxonomy of reasoning phases grounded in empirical measurement of representational structure:

Crystallization This phase characterizes legal reasoning at scale. The transition from 8B to 70B parameters induces a 45% collapse in global dimensionality ($d_{95} : 501 \rightarrow 274$) alongside a 31% increase in trajectory alignment ($0.72 \rightarrow 0.94$, $\sigma = 0.027$). This is not incremental improvement—it is structural transformation. The model does not merely reason better about law; it reasons differently, compressing the space of possible reasoning pathways into a low-dimensional, highly reproducible manifold. The global-to-local dimension ratio converges toward unity ($G/L \approx 0.98$), indicating that the 70B representation has achieved geometric efficiency: the manifold is maximally disentangled, with no wasted dimensions orthogonal to the intrinsic reasoning structure. Pilot validation with neural reasoning operators trained on 8B trajectories—achieving 63.6% accuracy on legal classification tasks, exceeding baselines by 10 percentage points—demonstrates that this geometric structure carries predictive power. The deeper Crystallization at 70B suggests this predictive capacity will scale with manifold disentanglement, a hypothesis that awaits direct experimental confirmation.

Liquidity This phase characterizes scientific reasoning across scales. Despite a $9 \times$ parameter increase, GPQA trajectories exhibit no dimensional compression ($d_{95} : 237 \rightarrow 235$) and maintain diffuse, exploratory geometry. Scale provides more parameters but does not reorganize the representational structure of scientific thought. This null result is as theoretically significant as the Crystallization finding: it demonstrates that the benefits of scale are not universal but depend on the match between model capacity and domain structure.

Lattice Formation This phase characterizes code reasoning. Scale increases cluster separation by 213% (silhouette: $0.133 \rightarrow 0.417$) and expands the number of identifiable strategies from 2 to 5, while maintaining moderate within-cluster alignment.

Programming, unlike law, does not converge to a single pathway; it organizes into discrete, well-separated strategic modes corresponding to recognizable problem-solving paradigms.

Beneath this domain-specific variation, we observe a universal constant: step-to-step coherence of approximately -0.4 persists across all domains, scales, and tasks. This oscillatory signature—reasoning trajectories that zig-zag rather than flow smoothly—appears to be an architectural invariant of transformer dynamics rather than a property of reasoning content. Any complete theory of transformer reasoning must account for this ubiquitous oscillation.

These findings carry immediate practical implications. Legal AI systems can exploit Crystallization for reliable deployment; the geometric compression and manifold disentanglement we observe suggest aggressive model compression may be achievable without capability loss. Scientific AI systems should not expect scale alone to improve reasoning quality; alternative approaches—retrieval augmentation, ensemble methods, or architectural innovations—may prove more effective. Code generation systems may benefit from explicit strategy detection, leveraging the Lattice structure to validate and route model outputs.

More broadly, our results suggest that the field’s understanding of scaling must become more nuanced. Aggregate scaling curves average over heterogeneous domain-specific effects. A model may exhibit emergent capabilities in some domains while remaining geometrically static in others. Understanding these disaggregated effects—predicting which domains will Crystallize at which scales—may be essential for efficient compute allocation and capability forecasting.

We close with a methodological observation. The geometric lens we have applied—analyzing dimensionality, alignment, clustering, and coherence of reasoning trajectories—reveals structure invisible to behavioral metrics alone. Two models with identical accuracy may occupy radically different geometric phases, implying different generalization properties, failure modes, and amenability to compression or acceleration. As language models are deployed in high-stakes domains, understanding not just what they output but how they traverse representational space during reasoning may prove essential for safety and reliability.

The geometry of thought is not uniform. Scale does not improve reasoning—it reshapes it, in ways that depend fundamentally on what the model is reasoning about. We have provided the first empirical map of this terrain. Much remains to be explored.

Data and Code Availability

All datasets used in this study (GSM8K, GPQA, HumanEval, CaseHOLD, and LexGLUE-SCOTUS) are publicly available under their respective licenses. We will release the extraction, geometry analysis, and operator/probe training code (including exact prompts, dataset subsampling manifests, and random seeds) upon acceptance; until then, materials are available to qualified researchers upon request. We do not redistribute model weights, and we do not bundle large raw hidden-state dumps; the release will include scripts to reproduce trajectory extraction from the original checkpoints.

References

1. L. Amsaleg, O. Chelly, T. Furion, S. Girard, M. E. Houle, K.-i. Kawarabayashi, and M. Nett. Estimating the intrinsic dimension using the correlation dimension. In *Proceedings of the 24th ACM International Conference on Information and Knowledge Management*, pages 103–112, 2015.
2. A. Ansuini, A. Laio, J. H. Macke, and D. Zoccolan. Intrinsic dimension of data representations in deep neural networks. *arXiv preprint arXiv:1905.12784*, 2019.
3. Y. Bahri, J. Kadmon, S. Ganguli, and J. Sohl-Dickstein. Statistical mechanics of deep learning. *Annual Review of Condensed Matter Physics*, 11:501–528, 2020.
4. I. Beltagy, M. E. Peters, and A. Cohan. Longformer: The long-document transformer. *arXiv preprint arXiv:2004.05150*, 2020.
5. Y. Bengio, A. Courville, and P. Vincent. Representation learning: A review and new perspectives. *IEEE Transactions on Pattern Analysis and Machine Intelligence*, 35(8):1798–1828, 2013.
6. M. Besta, N. Blach, A. Kubicek, R. Gerstenberger, L. Gianinazzi, J. Gajda, T. Lehmann, M. Podstawska, H. Nolle, A. Butler, et al. Graph of thoughts: Solving elaborate problems with large language models. *arXiv preprint arXiv:2308.09687*, 2024.
7. P. P. Brahma, D. Wu, and Y. She. Why deep learning works ii: The manifold entanglement limit. *arXiv preprint arXiv:1510.05202*, 2016.
8. C. Burns, H. Ye, D. Klein, and J. Steinhardt. Discovering latent knowledge in language models without supervision. *arXiv preprint arXiv:2212.03827*, 2023.

9. T. Cai, Y. Li, Z. Geng, H. Peng, J. D. Lee, D. Chen, and T. Dao. Medusa: Simple llm inference acceleration framework with multiple decoding heads. *arXiv preprint arXiv:2401.10774*, 2024.
10. J. D. Carson and A. Reisizadeh. A statistical physics of language model reasoning. *arXiv preprint arXiv:2506.04374*, 2025.
11. I. Chalkidis, A. Jana, D. Hartung, M. Bommarito, I. Androutsopoulos, D. M. Katz, and N. Aletras. Lexglue: A benchmark dataset for legal language understanding in english. In *Proceedings of the 60th Annual Meeting of the Association for Computational Linguistics (Volume 1: Long Papers)*, pages 4310–4330, 2022.
12. C. Chen, S. Borgeaud, G. Irving, J.-B. Lespiau, L. Sifre, and J. Jumper. Accelerating large language model decoding with speculative sampling. *arXiv preprint arXiv:2302.01318*, 2023.
13. M. Chen, J. Tworek, H. Jun, Q. Yuan, H. P. d. O. Pinto, J. Kaplan, H. Edwards, Y. Burda, N. Joseph, G. Brockman, et al. Evaluating large language models trained on code. *arXiv preprint arXiv:2107.03374*, 2021.
14. T. Chen and H. Chen. Universal approximation to nonlinear operators by neural networks. *IEEE Transactions on Neural Networks*, 6(4):911–917, 1995.
15. R. Child, S. Gray, A. Radford, and I. Sutskever. Generating long sequences with sparse transformers. *arXiv preprint arXiv:1904.10509*, 2019.
16. K. Cobbe, V. Kosaraju, M. Bavarian, M. Chen, H. Jun, L. Kaiser, M. Plappert, J. Tworek, J. Hilton, R. Nakano, et al. Training verifiers to solve math word problems. *arXiv preprint arXiv:2110.14168*, 2021.
17. T. Dettmers, M. Lewis, Y. Belkada, and L. Zettlemoyer. Llm.int8(): 8-bit matrix multiplication for transformers at scale. *arXiv preprint arXiv:2208.07339*, 2022.
18. N. Elhage, N. Nanda, C. Olsson, T. Henighan, N. Joseph, B. Mann, A. Askell, Y. Bai, A. Chen, T. Conerly, et al. A mathematical framework for transformer circuits. *Transformer Circuits Thread*, 2021.
19. E. Facco, M. d’Errico, A. Rodriguez, and A. Laio. Estimating the intrinsic dimension of datasets by a minimal neighborhood information. *Scientific Reports*, 7(1):12140, 2017.
20. W. Fedus, B. Zoph, and N. Shazeer. Switch transformers: Scaling to trillion parameter models with simple and efficient sparsity. *arXiv preprint arXiv:2101.03961*, 2022.
21. G. Feng, B. Zhang, Y. Gu, H. Ye, D. He, and L. Wang. Towards revealing the mystery behind chain of thought: A theoretical perspective. *arXiv preprint arXiv:2305.15408*, 2024.
22. E. Frantar and D. Alistarh. Sparsegpt: Massive language models can be accurately pruned in one-shot. *arXiv preprint arXiv:2301.00774*, 2023.
23. D. Ganguli, D. Hernandez, L. Lovitt, A. Askell, Y. Bai, A. Chen, T. Conerly, N. Dassarma, D. Drain, N. Elhage, et al. Predictability and surprise in large generative models. *arXiv preprint arXiv:2202.07785*, 2022.

24. B. Geshkovski, C. Letrouit, Y. Polyanskiy, and P. Rigollet. The emergence of clusters in self-attention dynamics. *arXiv preprint arXiv:2305.05465*, 2023.
25. J. Hoffmann, S. Borgeaud, A. Mensch, E. Buchatskaya, T. Cai, E. Rutherford, D. de Las Casas, L. A. Hendricks, J. Welbl, A. Clark, et al. Training compute-optimal large language models. *arXiv preprint arXiv:2203.15556*, 2022.
26. J. J. Hopfield. Neural networks and physical systems with emergent collective computational abilities. *Proceedings of the National Academy of Sciences*, 79(8):2554–2558, 1982.
27. J. Kaplan, S. McCandlish, T. Henighan, T. B. Brown, B. Chess, R. Child, S. Gray, A. Radford, J. Wu, and D. Amodei. Scaling laws for neural language models. *arXiv preprint arXiv:2001.08361*, 2020.
28. T. Kojima, S. S. Gu, M. Reid, Y. Matsuo, and Y. Iwasawa. Large language models are zero-shot reasoners. *arXiv preprint arXiv:2205.11916*, 2022.
29. N. Kovachki, Z. Li, B. Liu, K. Azizzadenesheli, K. Bhattacharya, A. Stuart, and A. Anandkumar. Neural operator: Learning maps between function spaces. *Journal of Machine Learning Research*, 24(89):1–97, 2023.
30. Y. Leviathan, M. Kalman, and Y. Matias. Fast inference from transformers via speculative decoding. *arXiv preprint arXiv:2211.17192*, 2023.
31. E. Levina and P. J. Bickel. Maximum likelihood estimation of intrinsic dimension. In *Advances in Neural Information Processing Systems*, volume 17, 2004.
32. B. Li, G. Deng, R. Chen, J. Yue, S. Zhang, Q. Zhao, L. Song, and L. Wen. Rema: A unified reasoning manifold framework for interpreting large language model. *arXiv preprint arXiv:2509.22518*, 2025.
33. Y. Li, F. Wei, C. Zhang, and H. Zhang. Eagle: Speculative sampling requires rethinking feature uncertainty. *arXiv preprint arXiv:2401.15077*, 2024.
34. Z. Li, N. Kovachki, K. Azizzadenesheli, B. Liu, K. Bhattacharya, A. Stuart, and A. Anandkumar. Fourier neural operator for parametric partial differential equations. *arXiv preprint arXiv:2010.08895*, 2021.
35. Z. Liu, Y. Wang, S. Vaidya, F. Ruehle, J. Halverson, M. Soljačić, T. Y. Hou, and M. Tegmark. KAN: Kolmogorov-arnold networks. *arXiv preprint arXiv:2404.19756*, 2024.
36. L. Lu, P. Jin, G. Pang, Z. Zhang, and G. E. Karniadakis. Learning nonlinear operators via DeepONet based on the universal approximation theorem of operators. *Nature Machine Intelligence*, 3(3):218–229, 2021.
37. N. Maheswaranathan, A. Williams, M. Golub, S. Ganguli, and D. Sussillo. Reverse engineering recurrent networks for sentiment classification reveals line attractor dynamics. *Advances in Neural Information Processing Systems*, 32, 2019.
38. J. Marin. Geometric analysis of reasoning trajectories: A phase space approach to understanding valid and invalid multi-hop reasoning in llms. *arXiv preprint arXiv:2410.04415*, 2024.
39. W. Merrill and A. Sabharwal. The expressive power of transformers with chain of thought. *arXiv preprint arXiv:2310.07923*, 2023.

40. N. Nanda, L. Chan, T. Lieberum, J. Smith, and J. Steinhardt. Progress measures for grokking via mechanistic interpretability. *arXiv preprint arXiv:2301.05217*, 2023.
41. H. Narayanan and S. Mitter. Sample complexity of testing the manifold hypothesis. In *Advances in Neural Information Processing Systems*, volume 23, 2010.
42. C. Olsson, N. Elhage, N. Nanda, N. Joseph, N. DasSarma, T. Henighan, B. Mann, A. Askell, Y. Bai, A. Chen, et al. In-context learning and induction heads. *Transformer Circuits Thread*, 2022.
43. P. Pope, C. Zhu, A. Abdelkader, M. Goldblum, and T. Goldstein. The intrinsic dimension of images and its impact on learning. *arXiv preprint arXiv:2104.08894*, 2021.
44. A. Power, Y. Burda, H. Edwards, I. Babuschkin, and V. Misra. Grokking: Generalization beyond overfitting on small algorithmic datasets. *arXiv preprint arXiv:2201.02177*, 2022.
45. B. Prystawski and N. D. Goodman. Why think step-by-step? reasoning emerges from the locality of experience. *arXiv preprint arXiv:2304.03843*, 2024.
46. M. Raissi, P. Perdikaris, and G. E. Karniadakis. Physics-informed neural networks: A deep learning framework for solving forward and inverse problems involving nonlinear partial differential equations. *Journal of Computational Physics*, 378:686–707, 2019.
47. S. Recanatesi, M. Farrell, G. Lajoie, S. Deneve, M. Rigotti, and E. Shea-Brown. The dimensionality of representations in the brain. *arXiv preprint arXiv:1906.12297*, 2019.
48. D. Rein, B. L. Hou, A. C. Stickland, J. Petty, R. Y. Pang, J. Dirani, J. Michael, and S. R. Bowman. Gpqa: A graduate-level google-proof q&a benchmark. *arXiv preprint arXiv:2311.12022*, 2023.
49. M. E. Sander, G. Pierre, M. Blondel, and G. Peyré. Sinkformers: Transformers with doubly stochastic attention. *arXiv preprint arXiv:2110.11773*, 2022.
50. A. M. Saxe, J. L. McClelland, and S. Ganguli. A mathematical theory of semantic development in deep neural networks. *Proceedings of the National Academy of Sciences*, 116(23):11537–11546, 2019.
51. R. Schaeffer, B. Miranda, and S. Koyejo. Are emergent abilities of large language models a mirage? *arXiv preprint arXiv:2304.15004*, 2023.
52. T. Schuster, A. Fisch, J. Gupta, M. Dehghani, D. Bahri, V. Q. Tran, Y. Tay, and D. Metzler. Confident adaptive language modeling. *arXiv preprint arXiv:2207.07061*, 2022.
53. D. Sussillo and O. Barak. Opening the black box: Low-dimensional dynamics in high-dimensional recurrent neural networks. *Neural Computation*, 25(3):626–649, 2013.
54. A. Turner, L. Thiergart, D. Udell, G. Leech, U. Mini, and M. MacDiarmid. Activation addition: Steering language models without optimization. *arXiv preprint arXiv:2308.10248*, 2023.

55. X. Wang, J. Wei, D. Schuurmans, Q. Le, E. Chi, S. Narang, A. Chowdhery, and D. Zhou. Self-consistency improves chain of thought reasoning in language models. *arXiv preprint arXiv:2203.11171*, 2023.
56. J. Wei, Y. Tay, R. Bommasani, C. Raffel, B. Zoph, S. Borgeaud, D. Yogatama, M. Bosma, D. Zhou, D. Metzler, et al. Emergent abilities of large language models. *arXiv preprint arXiv:2206.07682*, 2022.
57. J. Wei, X. Wang, D. Schuurmans, M. Bosma, B. Ichter, F. Xia, E. H. Chi, Q. V. Le, and D. Zhou. Chain-of-thought prompting elicits reasoning in large language models. *arXiv preprint arXiv:2201.11903*, 2022.
58. D. Wright and A. Gonzalez. Transformers as flows on the space of sequences. *arXiv preprint arXiv:2109.00634*, 2021.
59. S. Yao, D. Yu, J. Zhao, I. Shafran, T. L. Griffiths, Y. Cao, and K. Narasimhan. Tree of thoughts: Deliberate problem solving with large language models. *arXiv preprint arXiv:2305.10601*, 2023.
60. L. Zheng, N. Guha, B. R. Anderson, P. Henderson, and D. E. Ho. When does pretraining help? assessing self-supervised learning for law and the casehold dataset of 53,000+ legal holdings. In *Proceedings of the Eighteenth International Conference on Artificial Intelligence and Law (ICAIL '21)*. ACM, 2021.
61. A. Zou, L. Phan, S. Chen, J. Campbell, P. Guo, R. Ren, A. Pan, X. Yin, M. Mazeika, A.-K. Dombrowski, et al. Representation engineering: A top-down approach to ai transparency. *arXiv preprint arXiv:2310.01405*, 2023.